

PAPER

[View Article Online](#)
[View Journal](#) | [View Issue](#)Cite this: *Mater. Adv.*, 2022,
3, 409

A synergistic approach to achieving high conduction and stability of CsH₂PO₄/NaH₂PO₄/ZrO₂ composites for fuel cells

Dharm Veer,^a Pawan Kumar,^b *^a Deshraj Singh,^b Devendra Kumar^a and Ram S Katiyar^c

Solid acid composites of CsH₂PO₄/NaH₂PO₄/ZrO₂ with different weight ratios of CsH₂PO₄ (CDP), NaH₂PO₄ (SDP), and ZrO₂ were synthesized and characterized. The structure and morphology of the composites were investigated by XRD, FESEM, EDX, and FTIR techniques. The thermal stability and conduction were described for the solid acid composites using TGA, DTA, and conductivity measurements. NaH₂PO₄ increased the low-temperature conductivity of CDP by up to 1.5 orders of magnitude and ZrO₂ enhanced the conductivity above the transition temperatures. Additionally, the composites showed excellent stability. The superprotonic transition behavior was identified at temperatures from 220 to 270 °C. The conductivity of the composites was examined in air and under confined conditions and also their decomposition was investigated. Our findings suggest that NaH₂PO₄/ZrO₂ is an appropriate composite for achieving the high conductivity and stability of CDP.

Received 14th July 2021,
Accepted 16th October 2021

DOI: 10.1039/d1ma00612f

rsc.li/materials-advances

1. Introduction

In modern society, there is a huge demand for emerging ecology as a renewable energy source. Fuel cells are becoming an attractive renewable energy generation source.¹ New studies are based on the high ionic conductivity and good mechanical properties of solid acid electrolytes for fuel cells. Solid acid fuel cells operate at intermediate temperatures^{2–6} which generates ingenuity for other fuel cell technologies. The formula M_aH_b(XO₄)_c represents the solid acid electrolytes, where M = Cs, Na, Rb, Li, and NH₄; X = P, As, S, and Se; a, b, and c are integers.⁷ At least one phase transition in this family corresponds to an increase in proton conductivity.⁸ CsHPO₄, RbH₂PO₄, and CsH₂PO₄ are solid acid electrolytes, in which CsH₂PO₄ (CDP) is a widely studied solid acid with superprotonic conductivity at 230 °C. This material was used as an electrolyte for fuel cells and its applicability was evaluated in various electrochemical cell applications.^{9–13} The proton conductivity of CDP increases up to three orders of magnitude upon heating.¹⁴ At high temperatures, the cubic form of CDP has been observed as a superprotonic phase. The highest conductivity of CDP and its potential use as a solid electrolyte has gained

renewed interest.^{15–18} The dehydration of CDP can be suppressed sufficiently due to the increase in thermal stability above the phase transition temperature.¹⁹ A solid acid is mixed with other solid acids or oxides²⁰ to produce composites with higher conductivity values and improved thermal stability. NaH₂PO₄ (SDP) is an impressive material due to the high stability of sodium ions and potential technological applications.²¹ It is useful in food, water treatment, medicine, cement, and other fields.²² The conductivity of CDP increases up to 1 to 3 orders of magnitude by SDP at low temperatures.²³ For an SA-doped material, a higher proton conductivity of 5.28 × 10^{−2} S cm was observed at 90 °C and 98% relative humidity. The conductivity of CDP/ZrO₂ was observed to be 1.8 × 10^{−2} S cm^{−1} for 2000 min in confined nature.²⁴ The conductivity value of CDP/NaH₂PO₄/SiO₂ was found to be 0.9 × 10^{−2} S cm^{−1} at 150 °C.²⁵ The proton conductivity of MPOPS-1 was found to be 1.49 × 10^{−5} and 3.07 × 10^{−2} S cm at a temperature of 350 K under anhydrous and humid conditions, respectively.²⁶ The conductivity of solid acids is increased by doping highly dispersed inert oxides like ZrO₂, TiO₂, SiO₂, and Al₂O₃, which is significantly higher than that of the pure CDP.²⁷ ZrO₂ is a particular oxide due to its ability to absorb and retain water at elevated temperatures due to the effect of mechanical stabilization.^{28,29} This work is devoted to studying the structural, conductivity, and thermal properties of composite electrolytes CDP/SDP/ZrO₂. For this, XRD, FESEM, EDX, TGA, DTA, FTIR, and conductivity measurement studies have been performed.

^a Department of Physics, Gurukula Kangri (Deemed to be University), Haridwar-249404, India. E-mail: pksoniyal13@gmail.com^b Department of Physics K.G.K. College, Moradabad, M.J.P Rohilkhand University, Bareilly-243006, India^c Department of Physics, University of Puerto Rico, PR-00931, USA

2. Materials and methods

CDP was prepared according to the following reaction by mixing the combined reagents Cs_2CO_3 and H_3PO_4 in a molar ratio of 1 : 2



A measured amount of Cs_2CO_3 was dissolved in distilled water for the synthesis of CDP and then the mixture was stirred for 30 min to obtain a clear solution. Phosphoric acid was added drop by drop to the mixture by stirring continuously for 30 min. The solution was vacuum filtered to produce a white precipitate CDP. The solid layer was washed with acetone and then calcined at 150 °C for 2 h to remove residual water and after that ground to produce the CDP powder. In the production of SDP, we applied the same process as CDP and only Na_2CO_3 was used in place of Cs_2CO_3 . In the production of SDP, we implemented a process similar to CDP, using Na_2CO_3 in place of Cs_2CO_3 .

CDP was mixed mechanically with zirconium dioxide for $\text{CsH}_2\text{PO}_4/\text{ZrO}_2$ composites. Now the solid acid $\text{CsH}_2\text{PO}_4/\text{ZrO}_2$ was mixed with NaH_2PO_4 in a weight ratio by mechanical grinding. The mixture CDP/SDP/ ZrO_2 was dried at 150 °C for 14 h. Then, the resultant precipitate was ground to form a fine solid acid composite powder. The mixed powder was pressed for 15 minutes at 5–7 tons and room temperature to form pellets of 4 mm thickness and 12 mm diameter. The electrodes on the pellets were made of a high vacuum coating unit (Hind High Vacuum-12A 4D) and then sintered at 90 °C for 2 h. To confirm the identity of the samples, powder X-ray diffraction (XRD) patterns were collected in the 2θ range of 20–60 °C using a Bruker D8 Advance diffractometer. The data of EDX and FESEM were recorded using a FESEM-Quanta 200 FEG. The composite decomposition was identified by measuring the mass loss by thermogravimetric analysis (TGA), and differential thermal analysis (DTA) using the SII 6300 XStar with respect to the temperature. TGA/DTA was performed using the powder samples under an airflow of 200 mL min^{-1} at a rate of 10 °C min^{-1} from 35 to 500 °C. The impedance data were plotted on the real and imaginary axes to determine the proton conductivity value. The pellets were used to measure the ionic conductivity from room temperature to 300 °C. An LCR meter (Hikoki 3532-50) was used to measure the conductivity in the frequency range of 50 Hz to 4 MHz. The ionic conductivity value was calculated from the resistance value R plotted in the Arrhenius form using the following formula:

$$\sigma \text{ (S cm}^{-1}\text{)} = L \text{ (cm)} / A \text{ (cm}^2\text{)} R \text{ (}\Omega\text{)}$$

where R is the resistance, L is the thickness and A is the pellet area. The functional groups in the solid acid materials were identified by Fourier-transform infrared spectroscopy (FTIR). The spectrum of the composites between 400 and 4000 cm^{-1} waves was collected at room temperature with an FTIR 8400S (Shimadzu) spectrometer.

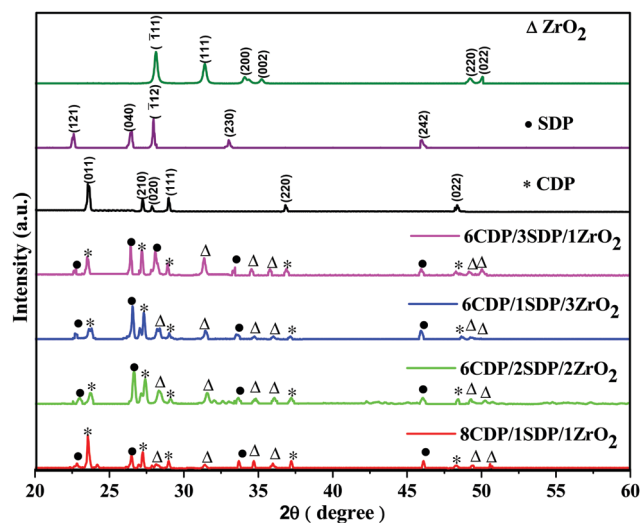


Fig. 1 X-ray diffraction patterns of CDP, SDP and ZrO_2 and their composites as prepared at room temperature.

3. Results and discussion

3.1. X-Ray diffraction (XRD)

The phase transitions in the range of $2\theta = 20^\circ$ to 60° of CDP, SDP, ZrO_2 , and their composites were analyzed by XRD as given in Fig. 1.

The sharp peaks appear at 23.54° , 27.13° , 27.90° , 28.96° , 36.73° , and 48.36° in the XRD spectra of CDP which were obtained similarly to JCPDS-761836. The peak at 23.54° corresponds to the Miller indices of the (011) plane which shows the monoclinic phase space group $P2_1/m$ for CDP. The monoclinic phase structure of CDP was found to exist from room temperature to 235 °C and the cubic phase from 240 to 280 °C. The partial dehydration of CDP occurred between the temperatures of 250 °C and 310 °C that produces $\text{Cs}_2\text{H}_2\text{P}_2\text{O}_7$ and CsPO_3 , respectively.³⁰ ZrO_2 and SDP were added to the solid acid composite to slow down the dehydration reaction. The peaks in the XRD of SDP were at 22.47° , 26.45° , 27.90° , 33.04° , and 45.93° , as detected using JCPDS-840112 with space group $P2_1/c$. ZrO_2 has peaks at 28.10° , 31.30° , 34.10° , 35.18° , 49.24° , and 50.01° with space group $P2_1/m$ using JCPDS-371484. All the peak values of the composites were observed to be similar to those of CDP, SDP, and ZrO_2 , which agree well with the JCPDS data. From the XRD results, it was found that CDP, SDP, and ZrO_2 have a monoclinic phase at room temperature. Tables 1 and 2(a–c) show the lattice parameters of the XRD and calculated values of the sharp peaks. The observed and calculated values confirm the XRD data and provide a reasonable true structure for all materials.

The intensity of the peaks decreases by changing the concentration of the additives of SDP and ZrO_2 , which suggests an increase in the degree of amorphousity in the composites. This phenomenon leads to ion diffusivity with ionic conductivity and stability. The XRD patterns confirm the crystalline structure of CDP, SDP, and ZrO_2 and their composites.



Table 1 Lattice parameters of CDP, SDP, and ZrO₂ in composites

| Material | JCPDS lattice parameters (Å) | CDP | SDP | ZrO ₂ | 8CDP/1SDP/1ZrO ₂ | 6CDP/2SDP/2ZrO ₂ | 6CDP/1SDP/3ZrO ₂ | 6CDP/3SDP/1ZrO ₂ |
|------------------|------------------------------|-------|--------|------------------|-----------------------------|-----------------------------|-----------------------------|-----------------------------|
| CDP | <i>a</i> = 7.9 | 7.533 | — | — | 7.530 | 7.561 | 7.518 | 7.555 |
| | <i>b</i> = 6.368 | 6.397 | — | — | 6.304 | 6.297 | 6.247 | 6.346 |
| | <i>c</i> = 4.872 | 4.698 | — | — | 4.992 | 4.622 | 4.615 | 4.676 |
| SDP | <i>a</i> = 6.808 | — | 6.788 | — | 6.924 | 6.683 | 6.620 | 6.613 |
| | <i>b</i> = 13.49 | — | 13.468 | — | 13.449 | 13.495 | 13.413 | 13.47 |
| | <i>c</i> = 7.331 | — | 7.335 | — | 7.353 | 7.312 | 7.342 | 7.370 |
| ZrO ₂ | <i>a</i> = 5.312 | — | — | 5.243 | 5.218 | 5.243 | 5.267 | 5.295 |
| | <i>b</i> = 5.212 | — | — | 5.196 | 5.156 | 5.277 | 5.190 | 5.217 |
| | <i>c</i> = 5.147 | — | — | 5.091 | 5.061 | 5.055 | 5.077 | 5.096 |

3.2. Fourier transform infrared spectroscopy (FTIR)

The IR spectra were recorded in the range of 400 cm⁻¹ to 4000 cm⁻¹ which are shown in Fig. 2(a and b).

The IR spectra of CDP and SDP showed the ABC bonds of OH at 2366 and 2333 cm⁻¹, respectively. The PO₄ components were assigned to the IR spectra at 900 to 1300 cm⁻¹ as the strong absorption bands. The P–O₂ asymmetric stretching modes in H₂PO₄⁻ anions were observed at 1117 cm⁻¹ and 1105 cm⁻¹. The well-separated peaks of CDP, SDP, and composites as observed in the IR spectra are given in Table 3.

No obvious change was observed in the IR spectra pattern of the composites when SDP was added, although this indicates a slight increase in the band frequency, lengthening of P–O–H, and shortening of P–O bonds which show an increase in conductivity.³¹ A decrease in the intensity of the composites was observed with the ZrO₂ increase that led to an increase in the amorphous region in the

mixed electrolytes which was in favor of the XRD results. The IR spectra of the composites provided significant changes in chemical composition, functionalization, and other changes.

3.3. Thermal analysis – TGA/DTA

The residual water content in the powder was studied by TGA/DTA analyses as shown in Fig. 3(a) and (b). The main weight losses of the powder were investigated at 10 °C min⁻¹ under an air atmosphere up to 500 °C. The total weight loss for CDP dehydration was found to be 8.73% at 500 °C, which is comparable to the theoretical value of CDP.³² CDP showed two endothermic transitions at 150 and 230 °C.³³ The weight loss of CDP was 1.95%, 3.13%, and 7.70% at 230 °C, 274 °C, and 373 °C, respectively. CDP was thermally stable up to 230 °C and indicates the endothermic effect associated with the superprotonic phase transition, which supports the conductivity measurement.

Table 2 Calculated values of the intense peaks for (a) CDP, (b) SDP, and (c) ZrO₂, with their composites of XRD

| Material | <i>hkl</i> | Peak position (2θ) | FWHM | Crystallite size (nm) | Microstrain $\epsilon \times 10^{-4}$ | Lattice spacing (Å) |
|-----------------------------|------------|--------------------|-------|-----------------------|---------------------------------------|---------------------|
| (a) | | | | | | |
| CDP | 400 | 48.328 | 0.279 | 31.132 | 11.134 | 1.881 |
| 8CDP/1SDP/1ZrO ₂ | 400 | 48.307 | 0.272 | 32.005 | 10.83 | 1.882 |
| 6CDP/2SDP/2ZrO ₂ | 400 | 48.091 | 0.186 | 46.729 | 7.417 | 1.890 |
| 6CDP/1SDP/3ZrO ₂ | 400 | 48.387 | 0.122 | 70.896 | 4.889 | 1.879 |
| 6CDP/3SDP/1ZrO ₂ | 400 | 48.295 | 0.306 | 28.420 | 12.196 | 1.882 |
| (b) | | | | | | |
| SDP | 121 | 22.57896302 | 0.191 | 42.252 | 8.20382 | 3.934 |
| | 002 | 24.2483439 | 0.261 | 31.034 | 11.16936 | 3.667 |
| | 210 | 27.06727031 | 0.161 | 50.585 | 6.85241 | 3.291 |
| 8CDP/1SDP/1ZrO ₂ | 121 | 22.81902 | 0.155 | 51.974 | 6.66928 | 3.893 |
| | 002 | 24.18712 | 0.105 | 76.835 | 4.51138 | 3.676 |
| | 210 | 27.23875 | 0.134 | 60.697 | 5.71086 | 3.271 |
| 6CDP/2SDP/2ZrO ₂ | 121 | 22.99207 | 0.377 | 21.465 | 16.14837 | 3.865 |
| | 002 | 24.3261 | 0.461 | 17.611 | 19.68215 | 3.656 |
| | 210 | 27.13686 | 0.191 | 42.753 | 8.10771 | 3.283 |
| 6CDP/1SDP/3ZrO ₂ | 121 | 22.92008064 | 0.410 | 19.727 | 17.5708 | 3.877 |
| | 002 | 24.22322418 | 0.201 | 40.389 | 8.58236 | 3.671 |
| | 210 | 26.91152218 | 1.06 | 7.703 | 44.99846 | 3.31 |
| 6CDP/3SDP/1ZrO ₂ | 121 | 22.59881374 | 0.241 | 33.513 | 10.34301 | 3.931 |
| | 002 | 24.12016947 | 0.416 | 19.481 | 17.79291 | 3.686 |
| | 210 | 27.19122348 | 0.132 | 61.627 | 5.62465 | 3.276 |
| (c) | | | | | | |
| ZrO ₂ | 120 | 38.542 | 0.238 | 35.240 | 9.836 | 2.333 |
| 8CDP/1SDP/1ZrO ₂ | 120 | 38.586 | 0.547 | 15.381 | 22.535 | 2.331 |
| 6CDP/2SDP/2ZrO ₂ | 120 | 38.701 | 0.310 | 27.140 | 12.772 | 2.324 |
| 6CDP/1SDP/3ZrO ₂ | 120 | 38.581 | 0.371 | 22.656 | 15.299 | 2.331 |
| 6CDP/3SDP/1ZrO ₂ | 120 | 38.469 | 0.444 | 18.945 | 18.296 | 2.338 |



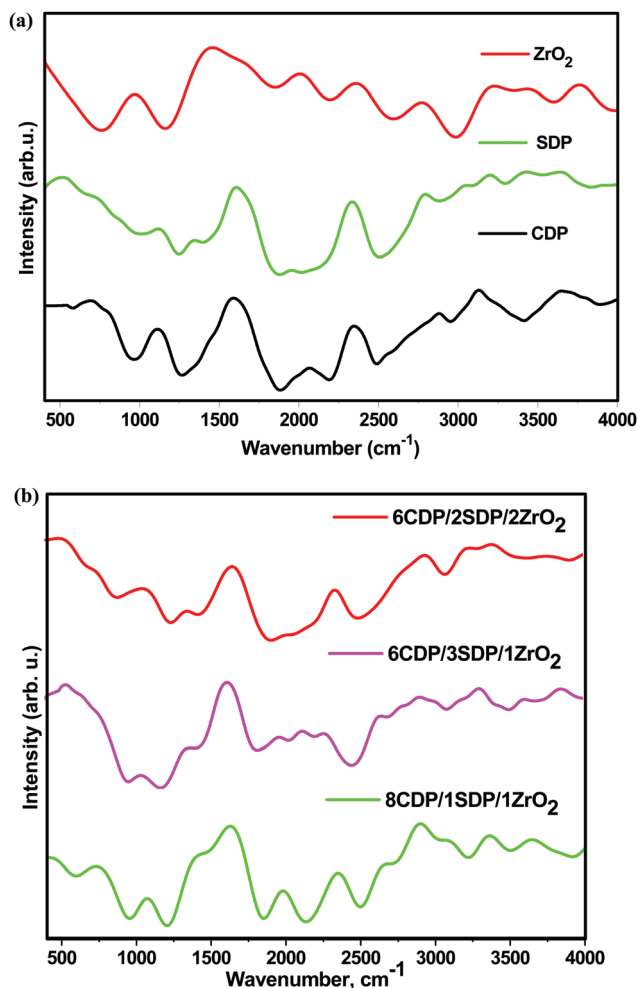


Fig. 2 Infrared spectra of pure CDP, SDP, and ZrO₂ (a) and their composites (b).

SDP showed a weight loss of 2.4%, 8.7%, and 16.28% at 65 °C, 217 °C, and 350 °C temperatures, respectively. SDP exhibited dehydration at several temperatures between 60 °C and 360 °C. The 60 °C condition in the SDP defines the presence of water molecules in it. SDP underwent dehydration in the other two stages: the first was with a 9% weight loss at 220 °C and the second at 350 °C with a 17% weight loss as shown in TGA. Therefore, adding SDP to the composites at low temperatures resulted in dehydration compared to pure CDP.³⁴

The endothermic events of pure CDP in the DTA curve were found at the temperatures of 150 °C, 230 °C, 310 °C, 320 °C, 340 °C, 350 °C, 360 °C, and 375 °C, respectively, which are shown in Fig. 3(b).

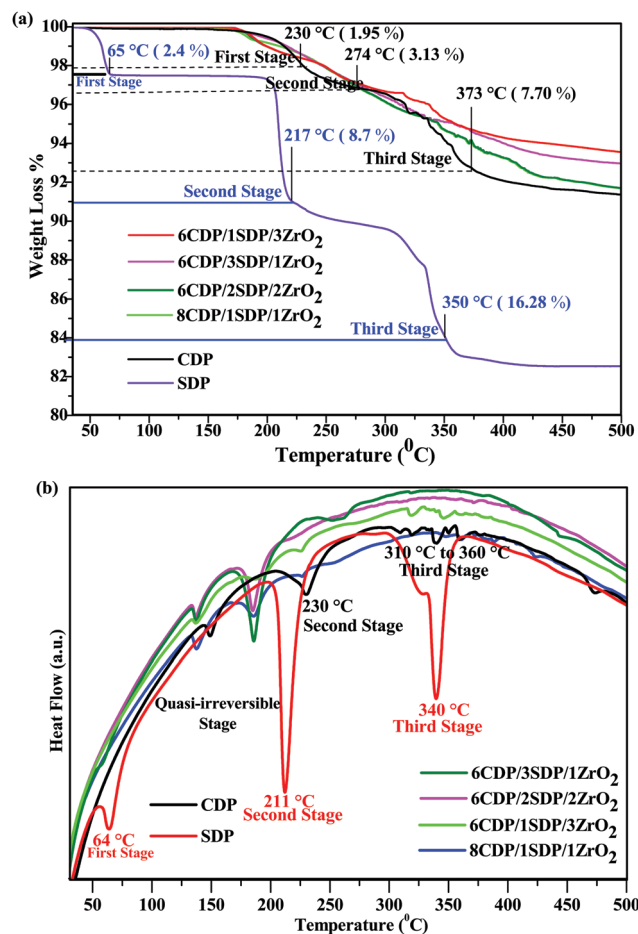


Fig. 3 (a) TGA and (b) DTA for CDP, SDP and their composites in an air flow of 200 mL min⁻¹.

The first stage in CDP was semi-irreversible at 150 °C due to the presence of CsH₅(PO₄)₂ and ferroelectric transition takes place.³⁵ All composites show similar endothermic events for CDP in DTA.

The endothermic effect in 6CDP/2SDP/2ZrO₂ was found to be invisible at 229 °C due to the transition of CDP. Three endothermic events of SDP in DTA were observed at 64 °C, 211 °C, and 340 °C temperatures. The TGA/DTA results for the composites indicate an improvement in the thermal stability of the CDP.

3.4. Conductivity

The electrical behavior of CDP and its composites was studied using the impedance spectroscopy technique as Nyquist plots, as shown in Fig. 4(a–d).

Table 3 Comparison of the functional groups present in the FTIR of CDP, SDP, and composite electrolytes

| Material | O–H stretching Medium sharp 3584–3700 | O–H stretching intermolecular bonded | | ABC bonds of OH | P–O ₂ stretching (asymmetric) |
|-----------------------------|---------------------------------------|--------------------------------------|---------------------|-----------------|--|
| | | Strong bond 3550–3200 | Weak bond 3200–2700 | | |
| CDP | 3672 | 3386 | 3148 | 2366 | 1117 |
| SDP | 3610 | 3419 | 3191 | 2333 | 1105 |
| 8CDP/1SDP/1ZrO ₂ | 3632 | 3369 | 2941 | 2341 | 1053 |
| 6CDP/1SDP/3ZrO ₂ | 3624 | 3357 | 2912 | 2349 | 1072 |
| 6CDP/2SDP/2ZrO ₂ | 3610 | 3387 | 2910 | 2343 | 1039 |

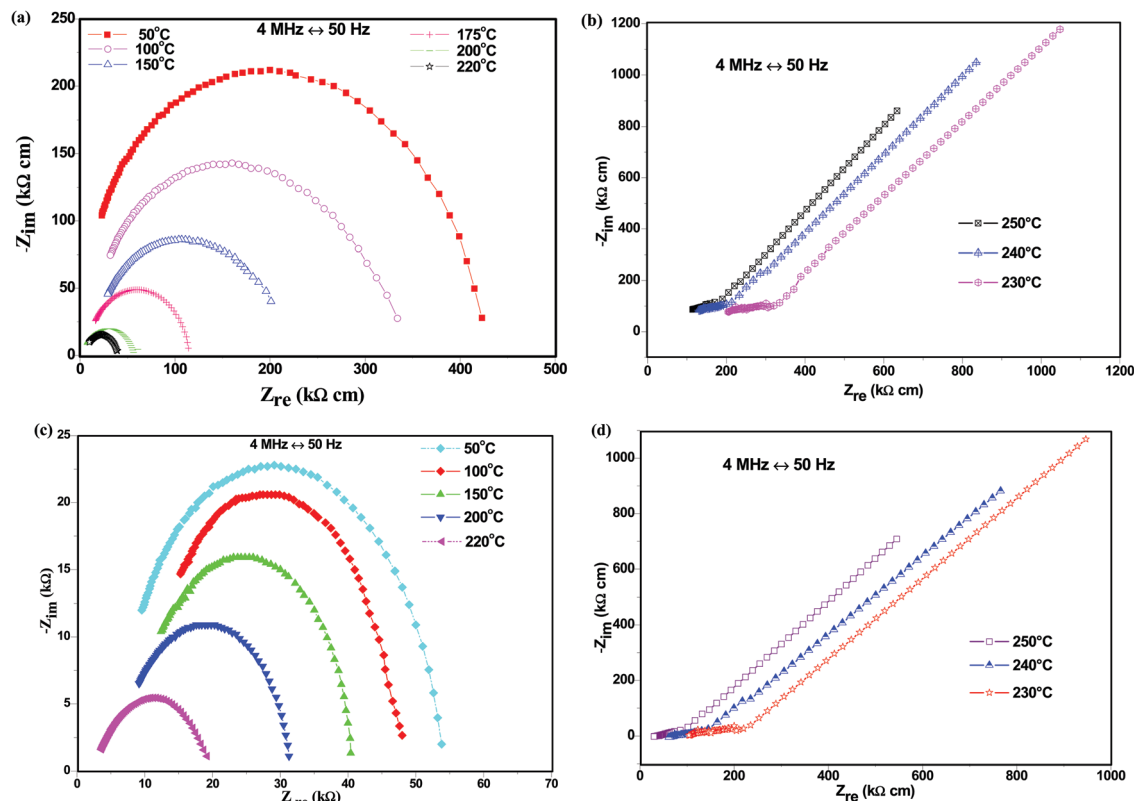


Fig. 4 The impedance measurement of CDP and its composites at different temperatures plotted in Nyquist plots. (a) CDP at 50 °C, 100 °C, 150 °C, 175 °C, 200 °C, and 220 °C. (b) CDP at 230 °C, 240 °C, and 250 °C. (c) 8CDP/1SDP/1ZrO₂ at 50 °C, 100 °C, 150 °C, 200 °C and 220 °C. (d) 8CDP/1SDP/1ZrO₂ at 230 °C, 240 °C, and 250 °C.

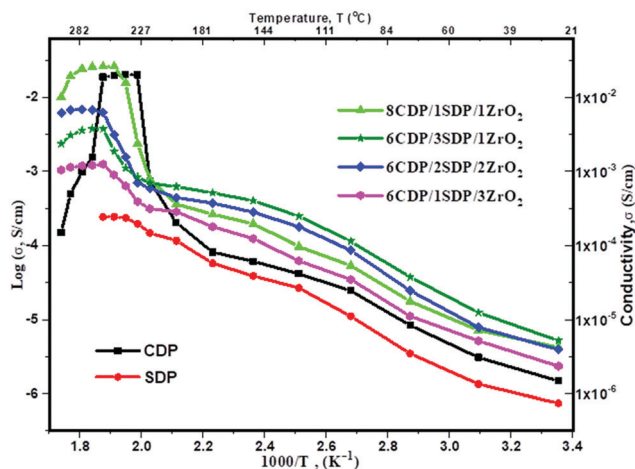


Fig. 5 Conductivity of CDP, SDP, and their four composites as a function of composition.

The appearance of semi-circular arcs was observed below the transition temperature due to the weakening of the grain boundaries, representing the processes at the electrolyte/electrode interface of the system.³⁶ The straight line represents an increase in ionic conductivity when heated above the transition temperature due to the monoclinic to the cubic phase transition, as observed in the undoped compound CsH₂PO₄. The arc radius

decreases with the increasing temperature due to electrode resistance, which shows an active thermal conductivity mechanism as shown in Fig. 4(b). The ionic conductivity of CDP was found to be maximum due to the high phosphorus content at the transition temperature which is determined by O–H concentration and free hydrogen bonding.³⁷ This result indicates an increase in the conductivity of CDP. Fig. 4(c and d) shows the impedance spectra below and above the transition temperatures for 8CDP/1SDP/1ZrO₂. The spectrum of 8CDP/1SDP/1ZrO₂ consists of a high-frequency region due to ionic conduction and a low-frequency region bounded by a straight line due to the electrode effect. The impedance spectra represent a high radius arc below the transition temperatures due to the strong hydrogen bond.³⁸ A decrease in the arc was observed due to the decrease in the resistive behavior of the material with the increase in the temperature as shown in Fig. 4(d). We have conducted analyses on the other composites and found the same behaviors. The impedance spectra of CDP and its composites exhibited almost the same characteristic that was also observed in the conductivity graph.

The conductivities of CDP, SDP, and their composites at different temperatures are presented in Fig. 5 and the values are given in Table 4.

The conductivities of CDP, SDP, and their composites were obtained between 25 °C and 300 °C temperatures. The conductivity value of CDP was found to be $2.008 \times 10^{-2} \text{ s cm}^{-1}$ at 240 °C, which is compared with the other results.³⁹ SDP is



Table 4 Conductivity values of CDP, SDP, and their composites at different temperatures

| Material | Highest conductivity value, σ (S cm ⁻¹) | Temperature during conductivity measurement (°C) |
|-----------------------------|--|--|
| CDP ³³ | 2.2×10^{-2} S cm ⁻¹ | 240 |
| CDP (pure) | 2.008×10^{-2} S cm ⁻¹ | 240 |
| SDP (pure) | 2.43×10^{-4} S cm ⁻¹ | 250 |
| 8CDP/1SDP/1ZrO ₂ | 2.23×10^{-2} S cm ⁻¹ | 250 |
| 8CDP/1SDP/1ZrO ₂ | 2.23×10^{-2} S cm ⁻¹ | 260 |
| CDP (pure) | 1.87×10^{-2} S cm ⁻¹ | 260 |
| 6CDP/3SDP/1ZrO ₂ | 3.76×10^{-3} S cm ⁻¹ | 260 |
| SDP (pure) | 2.42×10^{-4} S cm ⁻¹ | 260 |
| CDP (pure) | 1.94×10^{-2} S cm ⁻¹ | 250 |
| 6CDP/3SDP/1ZrO ₂ | 1.86×10^{-3} S cm ⁻¹ | 250 |
| 8CDP/1SDP/1ZrO ₂ | 1.57×10^{-2} S cm ⁻¹ | 240 |
| 6CDP/3SDP/1ZrO ₂ | 1.11×10^{-3} S cm ⁻¹ | 240 |
| SDP (pure) | 2.35×10^{-4} S cm ⁻¹ | 240 |
| CDP (pure) | 2.001×10^{-2} S cm ⁻¹ | 230 |
| 8CDP/1SDP/1ZrO ₂ | 2.38×10^{-3} S cm ⁻¹ | 230 |
| 6CDP/3SDP/1ZrO ₂ | 8.42×10^{-4} S cm ⁻¹ | 230 |
| SDP (pure) | 1.96×10^{-4} S cm ⁻¹ | 230 |
| 8CDP/1SDP/1ZrO ₂ | 7.84×10^{-4} S cm ⁻¹ | 220 |
| CDP (pure) | 7.44×10^{-4} S cm ⁻¹ | 220 |
| 6CDP/3SDP/1ZrO ₂ | 6.93×10^{-4} S cm ⁻¹ | 220 |
| SDP (pure) | 1.46×10^{-4} S cm ⁻¹ | 220 |
| 6CDP/3SDP/1ZrO ₂ | 6.20×10^{-4} S cm ⁻¹ | 200 |
| 8CDP/1SDP/1ZrO ₂ | 3.61×10^{-4} S cm ⁻¹ | 200 |
| CDP (pure) | 2.03×10^{-4} S cm ⁻¹ | 200 |
| SDP (pure) | 1.16×10^{-4} S cm ⁻¹ | 200 |
| 6CDP/3SDP/1ZrO ₂ | 4.02×10^{-4} S cm ⁻¹ | 150 |
| 8CDP/1SDP/1ZrO ₂ | 1.96×10^{-4} S cm ⁻¹ | 150 |
| CDP (pure) | 6.17×10^{-5} S cm ⁻¹ | 150 |
| SDP (pure) | 3.91×10^{-5} S cm ⁻¹ | 150 |

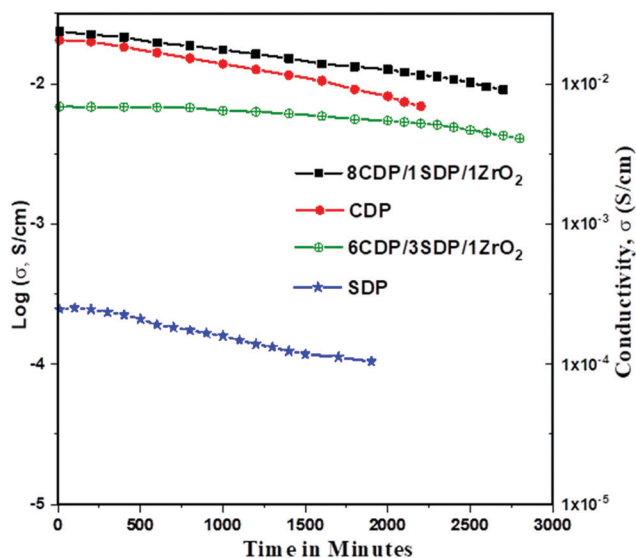


Fig. 6 Hermitically confined conductivity of CDP and its composites as a function of time.

known for its low conductivity which was measured to be 2.43×10^{-4} s cm⁻¹ at 250 °C. The range of conductivity values for all composites was observed from 7.88×10^{-6} s cm⁻¹ to 2.23×10^{-2} s cm⁻¹. 8CDP/1SDP/1ZrO₂ shows the highest conductivity from other composites which was found to be 2.23×10^{-2} S cm⁻¹ at 260 °C. We also found that the conductivity of solid acid composites at a high temperature

slightly increases due to the hydrophobicity and surface area of ZrO₂.⁴⁰ The conductivity of CDP/SDP/ZrO₂ increased to 1.5 orders of magnitude in the LT region and high temperature which was due to the structural disorder and deformation of the cation shape of ZrO₂.³¹

Furthermore, we investigated the time dependence of the ionic conductivity of CDP, SDP, and 8CDP/1SDP/1ZrO₂ under high hermetically confined conditions. The ionic conductivity of CDP is stable above 230 °C for long periods and composite 8CDP/1SDP/1ZrO₂ showed a high stable conductivity of 2.23×10^{-2} s cm⁻¹ for 42 hours as shown in Fig. 6, which is comparable to the other results.^{3,10,29,41,42}

To our knowledge, this is the first time that CDP, SDP, and ZrO₂ composites were observed for the stability and confined protonic conductivity of solid acid fuel cell electrolytes. We observed that adding SDP increases the conductivity and stability at lower temperatures of the composites. The conductivity results are comparable with the XRD and TGA/DTA data.

3.5. ESEM and EDX

The FESEM image shows the surface morphological investigations, and EDX spectroscopy was used to identify the chemical compositions of the material as shown in Fig. 7(a-c).

The pure CDP and SDP phases appeared as porous powder-like crystalline networks whereas the crystalline groups of phosphates appeared to cling to ZrO₂ inclusions as binders. A dense layer of the phosphate electrolyte was obtained from the doped oxide, which is used in the fuel cell.¹⁹ The obtained CDP material was composed of particles that are heterogeneous



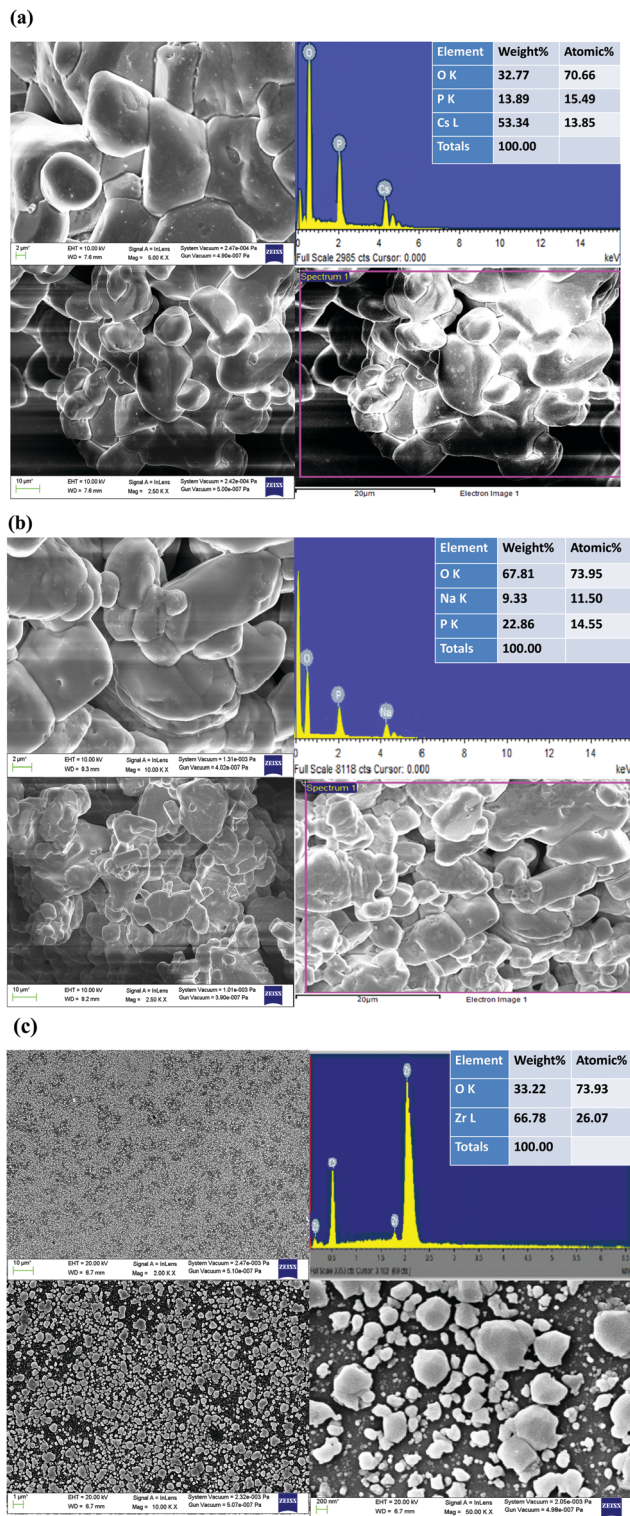


Fig. 7 FESEM images and EDX spectra of (a) CDP, (b) SDP, and (c) ZrO₂ nanoparticles.

and spherical in shape.⁴³ The chemical composition atomic % of Cs with P and O, Na with P and O, and Zr with O was calculated by EDX with their respective concentrations without any impurities. We found that the ion exchange reaction

between CDP, SDP, and ZrO₂ produces high proton conductivity by mechanical milling. The composition corresponded to that of CDP, SDP, and ZrO₂ according to the complex analysis of TGA, DTA, and EDX which is by the changes in the XRD patterns.

4. Conclusions

The composite electrolytes of CDP in weight ratio were analyzed within the intermediate temperature range. The solid solutions of CDP and its composites were confirmed by XRD at room temperature. The CDP and SDP dehydration peaks were observed up to 280 and 340 °C, respectively, as discussed in TGA and DTA, indicating that SDP is thermally unstable at higher temperatures. Our findings show that the superprotonic phase of CDP was stable using SDP at high temperatures. The superprotonic conduction nature was confirmed for CDP and its composites from Nyquist plots. A significant improvement in the thermal stability of the composites was shown by TGA/DTA. The range of conductivity values for composites was from $7.88 \times 10^{-6} \text{ s cm}^{-1}$ to $2.60 \times 10^{-2} \text{ s cm}^{-1}$, which increased to 1.5 orders of magnitude in lower and higher temperatures. 8CDP/1SDP/1ZrO₂ was found to be a promising material that showed the highest value of conductivity and stability in all composites which is comparable to those obtained by N. Mohammad *et al.*,²⁵ D. Singh *et al.*,²⁴ J. H. Leal *et al.*,¹⁰ and A. H. Jensen *et al.*, respectively.¹⁹ The time-dependent conductivity of 8CDP/1SDP/1ZrO₂ was achieved in 42 hours. The mechanism of proton transport within the composites was confirmed by FTIR analysis. Our results open up new possibilities for CDP and other solid acids that are attractive for use in phosphoric acid fuel cells.

Conflicts of interest

There are no conflicts to declare.

Acknowledgements

The authors thank the Materials Science Research Lab, Department of Physics, Gurukul Kangri (Deemed to be University), Haridwar (India), for providing facilities for the research work.

References

- 1 P. Bretzler, K. Köhler, A. V. Nikiforov, E. Christensen, R. W. Berg and N. J. Bjerrum, Efficient water splitting electrolysis on a platinum-free tungsten carbide electrocatalyst in molten CsH₂PO₄ at 350–390 °C, *Int. J. Hydrogen Energy*, 2020, **45**, 21262–21272, DOI: 10.1016/j.ijhydene.2020.05.145.
- 2 M. Z. Iqbal, Rafiuddin, Preparation, characterization, electrical conductivity and dielectric studies of Na₂SO₄ and V₂O₅ composite solid electrolytes, *Meas.: J. Int. Meas. Confed.*, 2016, **81**, 102–112, DOI: 10.1016/j.measurement.2015.12.008.



- 3 C. E. Botez, I. Martinez, A. Price, H. Martinez and J. H. Leal, Superprotonic CsH_2PO_4 in dry air, *J. Phys. Chem. Solids*, 2019, **129**, 324–328, DOI: 10.1016/j.jpcs.2019.02.001.
- 4 D. Aili, Y. Gao, J. Han and Q. Li, Acid-base chemistry and proton conductivity of CsHSO_4 , CsH_2PO_4 and their mixtures with N-heterocycles, *Solid State Ionics*, 2017, **306**, 13–19, DOI: 10.1016/j.ssi.2017.03.012.
- 5 R. Kikuchi, A. Ogawa, T. Matsuoaka, A. Takagaki, T. Sugawara and S. T. Oyama, Interfacial conduction mechanism of cesium hydrogen phosphate and silicon pyrophosphate composite electrolytes for intermediate-temperature fuel cells, *Solid State Ionics*, 2016, **285**, 160–164, DOI: 10.1016/j.ssi.2015.10.008.
- 6 A. D. Price, A. C. Aguilar, C. E. Botez and C. Li, Optical second harmonic generation imaging and X-ray diffraction of $\text{Cs}_{1-x}\text{Rb}_x\text{H}_2\text{PO}_4$ proton conductor series, *J. Appl. Phys.*, 2020, **127**, 193105, DOI: 10.1063/5.0006922.
- 7 H. Nakaya, M. Iwasaki, T. H. de Beauvoir and C. A. Randall, Applying cold sintering process to a proton electrolyte material: CsH_2PO_4 , *J. Eur. Ceram. Soc.*, 2019, **39**, 396–401, DOI: 10.1016/j.jeurceramsoc.2018.09.001.
- 8 G. Kim, J. M. Griffin, F. Blanc, S. M. Haile and C. P. Grey, Characterization of the dynamics in the protonic conductor CsH_2PO_4 by ^{17}O solid-state NMR spectroscopy and first-principles calculations: Correlating phosphate and protonic motion, *J. Am. Chem. Soc.*, 2015, **137**, 3867–3876, DOI: 10.1021/jacs.5b00280.
- 9 L. Navarrete, A. Andrio, S. Escolástico, S. Moya, V. Compañ and J. M. Serra, Protonic conduction of partially-substituted CsH_2PO_4 and the applicability in electrochemical devices, *Membranes*, 2019, **9**, 1–11, DOI: 10.3390/membranes9040049.
- 10 J. H. Leal, H. Martinez, I. Martinez, A. D. Price, A. G. Goos and C. E. Botez, Stability of the superprotonic conduction of $(1-x)\text{CsH}_2\text{PO}_4/x\text{SiO}_2$ ($0 \leq x \leq 0.3$) composites under dry and humid environments, *Mater. Today Commun.*, 2018, **15**, 11–17, DOI: 10.1016/j.mtcomm.2018.02.021.
- 11 A. A. Gaydamaka, V. G. Ponomareva and I. N. Bagryantseva, Phase composition, thermal and transport properties of the system based on the mono and dihydrogen phosphates of rubidium, *Solid State Ionics*, 2019, **329**, 124–130, DOI: 10.1016/j.ssi.2018.12.005.
- 12 B. Merinov, Proton transport mechanism, and pathways in the superprotonic phase of CsHSO_4 from experiment and theory, *Solid State Ionics*, 2012, **213**, 72–75, DOI: 10.1016/j.ssi.2011.07.012.
- 13 V. G. Ponomareva and I. N. Bagryantseva, The influence of $\text{Cs}_2\text{HPO}_4\cdot\text{H}_2\text{O}$ impurity on the proton conductivity and thermal properties of CsH_2PO_4 , *Solid State Ionics*, 2019, **329**, 90–94, DOI: 10.1016/j.ssi.2018.11.021.
- 14 Y. Taninouchi, N. Hatada, T. Uda and Y. Awakura, Phase Relationship of CsH_2PO_4 – CsPO_3 System and Electrical Properties of CsPO_3 , *J. Electrochem. Soc.*, 2009, **156**, B572, DOI: 10.1149/1.3086755.
- 15 S. Yoshimi, T. Matsui, R. Kikuchi and K. Eguchi, Temperature and humidity dependence of the electrode polarization in intermediate-temperature fuel cells employing $\text{CsH}_2\text{PO}_4/\text{SiP}_2\text{O}_7$ -based composite electrolytes, *J. Power Sources*, 2008, **179**, 497–503, DOI: 10.1016/j.jpowsour.2008.01.003.
- 16 C. E. Botez, J. D. Hermosillo, J. Zhang, J. Qian, Y. Zhao, J. Majzlan, R. R. Chianelli and C. Pantea, High-temperature phase transitions in CsH_2PO_4 under ambient and high-pressure conditions: A synchrotron X-ray diffraction study, *J. Chem. Phys.*, 2007, **127**, 194701, DOI: 10.1063/1.2804774.
- 17 G. Qing, R. Kikuchi, A. Takagaki, T. Sugawara and S. T. Oyama, CsH_2PO_4 /Polyvinylidene Fluoride Composite Electrolytes for Intermediate Temperature Fuel Cells, *J. Electrochem. Soc.*, 2014, **161**, 451–457, DOI: 10.1149/2.052404jes.
- 18 G. Qing, R. Kikuchi, A. Takagaki, T. Sugawara and S. T. Oyama, CsH_2PO_4 /Epoxy Composite Electrolytes for Intermediate Temperature Fuel Cells, *Electrochim. Acta*, 2015, **169**, 219–226, DOI: 10.1016/j.electacta.2015.04.089.
- 19 A. H. Jensen, Q. Li, E. Christensen and N. J. Bjerrum, Intermediate Temperature Fuel Cell Using $\text{CsH}_2\text{PO}_4/\text{ZrO}_2$ -Based Composite Electrolytes, *J. Electrochem. Soc.*, 2014, **161**, F72–F76, DOI: 10.1149/2.063401jes.
- 20 T. Rhimi, G. Leroy, B. Duponchel, K. Khirouni, S. Guermazi and M. Toumi, Electrical conductivity and dielectric analysis of NaH_2PO_4 compound, *Ionics*, 2018, **24**, 3507–3514, DOI: 10.1007/s11581-018-2494-6.
- 21 X. Zhang, C. Liu, W. Shen, Y. Ren, D. Li and H. Yang, Solubility and physic-chemical properties of NaH_2PO_4 in phosphoric acid, sodium chloride and their mixture solutions at $T = (298.15 \text{ and } 313.15) \text{ K}$, *J. Chem. Thermodyn.*, 2015, **90**, 185–192, DOI: 10.1016/j.jct.2015.06.038.
- 22 O. Rybalkina, K. Tsygurina, E. Melnikova, S. Mareev, I. Moroz, V. Nikonenko and N. Pismenskaya, Partial fluxes of phosphoric acid anions through anion-exchange membranes in the course of NaH_2PO_4 solution electrodialysis, *Int. J. Mol. Sci.*, 2019, **20**, 3593, DOI: 10.3390/ijms20143593.
- 23 N. Mohammad, A. B. Mohamad, A. A. H. Kadhum and K. S. Loh, Optimization of the composition and process parameter of $\text{CsH}_2\text{PO}_4/\text{NaH}_2\text{PO}_4/\text{SiO}_2$ solid acid composite via the Taguchi method, *Malaysian J. Anal. Sci.*, 2019, **23**, 109–115, DOI: 10.17576/mjas-2019-2301-13.
- 24 D. Singh, P. Kumar, J. Singh, D. Veer, A. Kumar and R. S. Katiyar, Structural, thermal and electrical properties of composites electrolytes $(1-x)\text{CsH}_2\text{PO}_4/x\text{ZrO}_2$ ($0 \leq x \leq 0.4$) for fuel cell with advanced electrode, *SN Appl. Sci.*, 2021, **3**, 1–7, DOI: 10.1007/s42452-020-04097-9.
- 25 N. Mohammad, A. B. Mohamad, A. A. H. Kadhum and K. S. Loh, Effect of silica on the thermal behaviour and ionic conductivity of mixed salt solid acid composites, *J. Alloys Compd.*, 2017, **690**, 896–902, DOI: 10.1016/j.jallcom.2016.08.188.
- 26 P. Bhanja, A. Palui, S. Chatterjee, Y. V. Kaneti, J. Na, Y. Sugahara, A. Bhaumik and Y. Yamauchi, Crystalline Porous Organic Polymer Bearing $-\text{SO}_3\text{H}$ Functionality for High Proton Conductivity, *ACS Sustainable Chem. Eng.*, 2020, **8**, 2423–2432, DOI: 10.1021/acssuschemeng.9b06234.
- 27 A. I. Baranov, V. V. Grebenev, A. N. Khodan, V. V. Dolbinina and E. P. Efremova, Optimization of superprotonic acid



- salts for fuel cell applications, *Solid State Ionics*, 2005, **176**, 2871–2874, DOI: 10.1016/j.ssi.2005.09.018.
- 28 C. Gautam, J. Joyner, A. Gautam, J. Rao and R. Vajtai, Zirconia based dental ceramics: structure, mechanical properties, biocompatibility and applications, *Dalton Trans.*, 2016, **45**, 19194–19215, DOI: 10.1039/c6dt03484e.
 - 29 M. F. R. P. Alves, S. Ribeiro, P. A. Suzuki, K. Strecker and C. dos Santos, Effect of Fe_2O_3 addition and sintering temperature on mechanical properties and translucence of zirconia dental ceramics with different Y_2O_3 content, *Mater. Res.*, 2021, **24**(2), DOI: 10.1590/1980-5373-MR-2020-0402.
 - 30 J. Otomo, N. Minagawa, C. J. Wen, K. Eguchi and H. Takahashi, Protonic conduction of CsH_2PO_4 and its composite with silica in dry and humid atmospheres, *Solid State Ionics*, 2003, **156**, 357–369, DOI: 10.1016/S0167-2738(02)00746-4.
 - 31 V. V. Martsinkevich and V. G. Ponomareva, Double salts $\text{Cs}_{1-x}\text{M}_x\text{H}_2\text{PO}_4$ ($\text{M} = \text{Na}, \text{K}, \text{Rb}$) as proton conductors, *Solid State Ionics*, 2012, **225**, 236–240, DOI: 10.1016/j.ssi.2012.04.016.
 - 32 T. Anfimova, A. H. Jensen, E. Christensen, J. O. Jensen, N. J. Bjerrum and Q. Li, $\text{CsH}_2\text{PO}_4/\text{NdPO}_4$ Composites as Proton Conducting Electrolytes for Intermediate Temperature Fuel Cells, *J. Electrochem. Soc.*, 2015, **162**, 436–441, DOI: 10.1149/2.0671504jes.
 - 33 S. Hosseini, A. B. Mohamad, A. H. KaHum and W. R. Wan Daud, Thermal analysis of CsH_2PO_4 nanoparticles using surfactants CTAB and F-68, *J. Therm. Anal. Calorim.*, 2010, **99**, 197–202, DOI: 10.1007/s10973-009-0132-2.
 - 34 Z. Li and T. Tang, High-temperature thermal behaviors of XH_2PO_4 ($\text{X} = \text{Cs}, \text{Rb}, \text{K}, \text{Na}$) and LiH_2PO_3 , *Thermochim. Acta*, 2010, **501**, 59–64, DOI: 10.1016/j.tca.2010.01.010.
 - 35 G. V. Lavrova and V. G. Ponomareva, Intermediate-temperature composite proton electrolyte $\text{CsH}_5(\text{PO}_4)_2/\text{SiO}_2$: Transport properties versus oxide characteristic, *Solid State Ionics*, 2008, **179**, 1170–1173, DOI: 10.1016/j.ssi.2008.01.003.
 - 36 V. G. Ponomareva and E. S. Shutova, Electrical conductivity and structural properties of proton electrolytes based on CsH_2PO_4 and silicophosphate matrices with low phosphorus content, *Inorg. Mater.*, 2014, **50**, 1056–1062, DOI: 10.1134/S0020168514100136.
 - 37 A. Matsuda, T. Kanzaki, Y. Kotani, M. Tatsumisago and T. Minami, Proton conductivity and structure of phospho-silicate gels derived from tetraethoxysilane and phosphoric acid or triethylphosphate, *Solid State Ionics*, 2001, **139**, 113–119, DOI: 10.1016/S0167-2738(00)00819-5.
 - 38 A. A. Gaydamaka, I. N. Bagryantseva and V. G. Ponomareva, Thermal properties, proton conductivity and vibration study of $\text{Rb}_2\text{HPO}_4 \cdot 2\text{H}_2\text{O}$, *J. Therm. Anal. Calorim.*, 2018, **133**, 1121–1127, DOI: 10.1007/s10973-018-7402-9.
 - 39 S. M. Haile, C. R. I. Chisholm, K. Sasaki, D. A. Boysen and T. Uda, Solid acid proton conductors: from laboratory curiosities to fuel cell electrolytes, *Faraday Discuss.*, 2006, **134**, 17–39, DOI: 10.1039/B604311A.
 - 40 N. Mohammad, A. B. Mohamad, A. A. H. Kadhum and L. K. Shyuan, Conductivity and thermal stability of solid acid composites $\text{CsH}_2\text{PO}_4/\text{NaH}_2\text{PO}_4/\text{SiO}_2$, *Malaysian J. Anal. Sci.*, 2016, **20**, 633–641, DOI: 10.17576/mjas-2016-2003-24.
 - 41 S. Wang, J. Otomo, M. Ogura, C. J. Wen, H. Nagamoto and H. Takahashi, Preparation and characterization of proton-conducting $\text{CsHSO}_4\text{-SiO}_2$ nanocomposite electrolyte membranes, *Solid State Ionics*, 2005, **176**, 755–760, DOI: 10.1016/j.ssi.2004.10.013.
 - 42 D. Singh, J. Singh, P. Kumar, D. Veer, D. Kumar, R. S. Katiyar, A. Kumar and A. Kumar, The Influence of TiO_2 on the Proton Conduction and Thermal Stability of CsH_2PO_4 Composite Electrolytes, *S. Afr. J. Chem. Eng.*, 2021, **37**, 227–236, DOI: 10.1016/j.sajce.2021.06.006.
 - 43 I. N. Bagryantseva, A. A. Gaydamaka and V. G. Ponomareva, Intermediate temperature proton electrolytes based on cesium dihydrogen phosphate and Butvar polymer, *Ionics*, 2020, **26**, 1813–1818, DOI: 10.1007/s11581-020-03505-9.

